ACS EARTH AND SPACE CHEMISTRY

http://pubs.acs.org/journal/aesccq

Article

Metal Substitution-Induced Reducing Capacity of Magnetite Coupled with Aqueous Fe(II)

Ying Li, Gaoling Wei, Xiaoliang Liang,* Caihua Zhang, Jianxi Zhu, and Yuji Arai

Cite This: *ACS Earth Space Chem.* 2020, 4, 905–911

Read Online

ACCESS | Metrics & More | Article Recommendations | Supporting Information

ABSTRACT: Aqueous Fe(II) ($Fe(II)_{aq}$) effectively magnifies the reducibility of magnetite toward environmental substances. In natural magnetite, isomorphous substitution by foreign metals is ubiquitous, and Zn^{2+} and Co^{2+} have been reported to positively improve the reducing capacity of magnetite coupled with $Fe(II)_{aq}$. Though most metal ions significantly alter the surface properties of magnetite, their effects on the reactivity of magnetite coupled with $Fe(II)_{aq}$ have rarely been systematically compared, resulting in the ambiguity of constraint mechanism and controlling factors. Herein, magnetites ($Fe_{3-x}M_xO_4$, M = Co^{2+}, Mn^{2+}, Zn^{2+}, Mg^{2+}, Cr^{3+}, and Al^{3+}) with similar substitution level ($x \approx 0.5$) were synthesized, characterized, and tested for the reduction of nitrobenzene (NB) in the presence of $Fe(II)_{aq}$. Both the reduction kinetics and the extent of electron transfer illustrated the positive effect of divalent metals but the negative effect of trivalent ones. Such distinct effects were further correlated to the physiochemical properties and microstructure of magnetite by the Pearson analysis. The active-site density and electrical conductivity of magnetite were critical factors determining the reduction performance of the coupled system. Specifically, Co, Mn, Zn, and Mg increased the active-site density and accordingly the adsorption capacity of $Fe(II)_{aq}$. Moreover, the octahedral Mn and Co with thermodynamically favorable redox pairs, i.e., Co^{2+}/Co^{3+} and Mn^{2+}/Mn^{3+}, accelerated electron exchange, giving rise to the increase of electrical conductivity. The tetrahedral Zn^{2+} induced the oxidation of octahedral Fe^{2+} to Fe^{3+}, which also promoted the electron transfer. These results shed light on the role of natural magnetite and its impact on the fate of nitroaromatic compounds in anoxic environments.

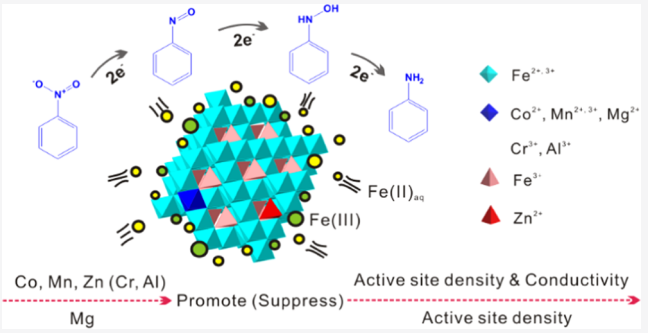

KEYWORDS: *magnetite, isomorphous substitution, aqueous Fe(II), reduction, electron transfer, Fe(II) adsorption*

INTRODUCTION

In anoxic environments, e.g., paddy soils and sediments, the reduction over iron (oxyhydr)oxide surface is a primary process controlling the migration and transformation of environmental substances.[1,2] Among iron oxides, magnetite, which is formed via the reduction of Fe^{3+} oxides by dissimilatory iron-reducing bacteria (DIRB) or the oxidation of ferrous mineral and iron metal, is one of the Fe^{2+}-bearing minerals.[3,4] Generally, structural Fe^{2+} is a strong electron donor.[5,6] Therefore, magnetite has been widely applied in anoxic remediation to effectively reduce organics (e.g., (chloro)nitrobenzene and carbon tetrachloride),[4,7] heavy metals (e.g., Cr(VI) and Hg(II)),[8,9] and radionuclides (e.g., U(VI)).[10] However, with reduction reaction proceeding, partial Fe^{2+} in magnetite is oxidized, resulting in the loss of reduction capacity. Interestingly, $Fe(II)_{aq}$, generated through the reduction of ferric oxides by DIRB,[11] recovers the reducibility of magnetite through the adsorption and electron transfer from adsorbed Fe(II) to oxidized magnetite.[12,13] This magnifies the role of magnetite as an effective reductant in natural environments.

In recent years, the coupling between magnetite and $Fe(II)_{aq}$ (magnetite/$Fe(II)_{aq}$ system) and the resulting reducibility have attracted great interest.[10,14,15] The reduction process of environmental substance by coupled system follows two steps: (1) adsorption of $Fe(II)_{aq}$ on the magnetite surface and (2) electron transfer from adsorbed Fe(II) and magnetite to environmental substances. Thus, the structural character and surface properties of magnetite probably dominate the reducing capacity of coupled system. Magnetite has an inverse-spinel structure, where both Fe^{2+} and Fe^{3+} occupy the octahedral sites and another equivalence Fe^{3+} occupies the tetrahedral sites. In most nature environments, iron ions in magnetite can be isomorphously substituted by various metal ions, e.g., divalent (e.g., Co^{2+}, Mn^{2+}, Mg^{2+}, and Zn^{2+}),[16−18] trivalent (e.g., Al^{3+} and Cr^{3+}),[19,20] and tetravalent (Ti^{4+}) ions.[16]

Received: April 7, 2020
Revised: May 12, 2020
Accepted: May 15, 2020
Published: May 15, 2020

Table 1. Chemical Analysis and Physicochemical Properties of $Fe_{3-x}M_xO_4$ Samples

sample	M/Fe (molar ratio)	ion	occupancy	ionic radius (Å)	a_0 (Å)	crystal size (nm)	specific surface area ($m^2\ g^{-1}$)	active-site density (10^{20} site g^{-1})	pH_{pzc}	conductivity ($\Omega^{-1}\ cm^{-1}$)
Mag	0	Fe^{+2}	octahedron	0.78[23]	8.394	14.1	74	2.1	6.7	1.54×10^4
		Fe^{+3}	octahedron	0.64[23]						
		Fe^{+3}	tetrahedron	0.49[18]						
Mag-Mn	0.17	Mn^{+2}	octahedron	0.81[40]	8.476	14.4	60	4.2	7.0	3.20×10^5
		Mn^{+3}	octahedron	0.65[41]						
Mag-Co	0.20	Co^{+2}	octahedron	0.74[40]	8.379	12.8	83	4.5	6.8	5.21×10^5
Mag-Zn	0.20	Zn^{+2}	tetrahedron	0.60[18]	8.425	11.8	89	4.0	7.1	1.04×10^5
Mag-Mg	0.20	Mg^{+2}	octahedron	0.72[42]	8.385	11.0	107	2.8	6.9	0.97×10^4
Mag-Cr	0.18	Cr^{+3}	octahedron	0.63[43]	8.378	9.6	154	2.0	6.8	1.44×10^4
Mag-Al	0.19	Al^{+3}	octahedron	0.57[41]	8.368	10.2	120	1.5	6.7	1.13×10^4

Previous studies have revealed that the isomorphous substitution of metals in magnetite remarkably changed its physiochemical properties and microstructure and accordingly altered its surface reactivity.[16,20,21] On the one hand, owing to the difference in ionic radius, the substitution of Co^{2+} and Mn^{2+} for Fe^{2+} significantly increases the active-site density of magnetite, giving rise to the increase in the adsorption capacity.[20,22] This probably promotes the adsorption of $Fe(II)_{aq}$. On the other hand, redox-active metals (e.g., Mn^{2+}/Mn^{3+} and Co^{2+}/Co^{3+}) improve the Fenton reactivity of magnetite, by accelerating the electron transfer in the spinel structure.[21,22] Similarly, they might speed up the electron transfer among adsorbed Fe(II), magnetite, and environmental substance. Thus, some substitutions could enhance or suppress the reactivity of magnetite/$Fe(II)_{aq}$ system. This has been verified in our previous study, where Zn^{2+} and Co^{2+} substitutions generally promoted the reduction of (chloro)-nitrobenzene.[23,24] However, to the best of our knowledge, for most substituting metal ions, their effects on the reducing capacity of magnetite/$Fe(II)_{aq}$ system have not been systematically compared, resulting in the ambiguity of constraint mechanism and controlling factors.

The objective of this study was to investigate the effects of metal (Co, Mn, Zn, Mg, Cr, and Al) substitution in magnetite on the reducing capacity of magnetite/$Fe(II)_{aq}$ system and the constrain mechanism. These metals are common foreign metals in natural magnetite, which is ubiquitously distributed in soils, sediments, and rocks.[17,25] Nitrobenzene that is widely used as a probe in reduction studies was chosen to test the reducing capacity of different substituted magnetite coupled with $Fe(II)_{aq}$.[26,27] The reducing capacity of different magnetites coupled with $Fe(II)_{aq}$ was compared by the reaction rate constant, k_{obs}, and the extent of electron transfer. Pearson analysis was also performed to distinguish the major and minor factors controlling the reduction reaction.

MATERIALS AND METHODS

Magnetite Synthesis. The metal (Co, Mn, Zn, Mg, Cr, and Al)-substituted magnetite samples $Fe_{3-x}M_xO_4$ were synthesized using a coprecipitation method.[28] Suitable amounts of $FeCl_2{\cdot}4H_2O$, $FeCl_3{\cdot}6H_2O$, and corresponding chlorides of substituting cations (i.e., $CoCl_2{\cdot}6H_2O$, $MnCl_2{\cdot}4H_2O$, $ZnCl_2$, $MgCl_2{\cdot}6H_2O$, $CrCl_3{\cdot}6H_2O$, and $AlCl_3$) were dissolved in 400 mL of deionization water (total cation concentration = 0.3 mol L^{-1}), followed by the addition of 4.0 mL of 6.0 mol L^{-1} HCl and several drops of hydrazine hydrate to prevent hydroxide precipitation and ferrous oxidation. Then, the solution was dropwise titrated with a NaOH solution (4.0 mol L^{-1}, 210 mL) with vigorous stirring. After mixing, the reaction was maintained at 90 °C for 5 h to improve the growth of particles. The solution was purged by N_2 during the whole process to prevent ferrous oxidation. The particles were separated by centrifugation, washed with deionization water, and then centrifuged again. After washing five times, the samples were collected, dried in a freeze dryer for 24 h, ground, and sieved through a 200-mesh screen.

The contents of Fe and substituting metals in $Fe_{3-x}M_xO_4$ were analyzed on an Agilent 7700X inductively coupled plasma mass spectrometer (ICP-MS) after complete dissolution in a 6.0 mol L^{-1} HCl solution in an anaerobic glovebox. The x value in $Fe_{3-x}M_xO_4$ was calculated based on eq 1

$$x = \frac{3 \times 55.85 \times C_M}{M \times C_{Fe} + 55.85 \times C_M} \quad (1)$$

where M is the molar mass of substituting cations and C_{Fe} and C_M are the contents of Fe and substituting cations in synthetic $Fe_{3-x}M_xO_4$, respectively. The molar ratio of Fe and substituting metals was about 5:1 (Tables 1 and S1). The obtained magnetites were labeled as Mag, Mag-Co, Mag-Mn, Mag-Zn, Mag-Mg, Mag-Cr, and Mag-Al.

Magnetite Characterization. X-ray diffraction (XRD) patterns were obtained on a Bruker D8 Advance diffractometer with Cu Kα (40 kV and 40 mA) radiation source recording in a 2θ range of 10−80° at a step of 3° min^{-1}. The lattice parameter a_0 was calculated from the reflections (111), (220), (311), (400), (511), and (440) by the Nelson-Riley method. The Brunauer−Emmett−Teller (BET) specific surface area (SSA) was measured by N_2 adsorption on a Micromeritics ASAP 2020 instrument. The active-site density and the point of zero charge (PZC) of magnetite were analyzed by an acid/base titration method on a Mettler Toledo ET18 (Text S1). The electrical conductivity was analyzed on a PPMS-9 instrument. The ^{57}Fe Mössbauer spectra were detected on a Web Research, Inc. spectrometer at room temperature. The spectrometer with a 50 mCi ^{57}Co source dispersed as 10 wt % in a thin Rh foil was equipped with a Janis Model SHE-850-5 closed-cycle cryostat under triangular waveform mode. Spectra

https://dx.doi.org/10.1021/acsearthspacechem.0c00089
ACS Earth Space Chem. 2020, 4, 905−911

were calibrated by a 7 μm iron foil under the same measurement condition.

Batch Reduction Tests. The reduction of NB was conducted in an anaerobic glovebox (O_2(g) < 0.1 ppm, 25 °C) to prevent the oxidation of $Fe(II)_{aq}$ and magnetite. pH was controlled at 7.2 using a 3-(*N*-morpholino)-propanesulfonic acid (MOPS) buffer solution (0.5 mol L^{-1}, 10% by volume) to exclude the formation of $Fe(OH)_2$ precipitation at pH > 8.0 and the invalid adsorption of $Fe(II)_{aq}$ on the $Fe_{3-x}M_xO_4$ surface at pH lower than pH_{pzc} (6.7−7.1, Table 1).[4,13,23] The MOPS with pK_a of 7.2 was chosen as a buffer solution, which was often selected in previous studies.[4,13] A stock $Fe(II)_{aq}$ solution (2 mL, 0.2 mol L^{-1}, pH 1.0) was introduced into the $Fe_{3-x}M_xO_4$ suspension (1.0 g L^{-1}, 200 mL), followed by shaking at 560 rpm for 60 min to achieve equilibrium. Then, 2.0 mL of an NB stock solution (1.0 g L^{-1} in methanol) was added to initiate the reduction experiments. At each sampling time, 1 mL of aliquot was taken and immediately filtered through a hydrophilic polytetrafluoroethylene (PTFE) syringe filter (0.22 μm, Anpel) for chromatography analysis.

The concentrations of NB and its reduction products, i.e., nitrosobenzene, hydroxylamine, and aniline, were analyzed by high-performance liquid chromatography (HPLC, LC-20A, Shimadzu, Japan) with an ultraviolet−visible (UV−vis) detector at 254 nm, as described in the literature.[23] The concentration of $Fe(II)_{aq}$ was traced by phenanthroline method.[29] The total Fe content was measured after reducing Fe(III) to Fe(II) by a 10% hydroxylamine hydrochloride solution.[29]

Data Analysis. The Pearson correlation analysis was conducted to assess the associations among all of the assigned variables. The linear regression function analysis was performed by applying the stepwise selection procedures in SPSS V13.0. The extent of electron transfer and reaction rate constant k_{obs} were defined as efficiency response variables. The physicochemical properties, including electrical conductivity, pH of the point of zero charge (pH_{pzc}), $Fe(II)_{aq}$ adsorption capacity, active-site density, SSA, and crystal size, were expressed as potential influence variables.

RESULTS AND DISCUSSION

Composition, Structure, and Surface Properties. The chemical compositions of $Fe_{3-x}M_xO_4$ obtained from the chemical analysis indicated that the substitution level in $Fe_{3-x}M_xO_4$ was essentially the same, as the molar ratio of substituting metal to iron was close to 0.2 (Tables 1 and S1). This facilitated the comparison among the studied metals for their effects on the reactivity of coupled system.

The XRD patterns of $Fe_{3-x}M_xO_4$ (Figure 1) corresponded well to the standard card of magnetite (JCPDS: 19-0629), without observable diffractions related to substituting metal oxides. Thus, all of the synthetic samples had a spinel structure, where substituting metal cations entered the structure of magnetite rather than forming their oxides. For some samples, i.e., Mag-Mg and Mag-Zn, the diffraction peaks at ca. 31.6 and 45.5° appeared, attributing to the NaCl formed from the reagents in magnetite synthesis, i.e., sodium hydroxide and chloride salts. After substitution, the diffraction peak of magnetite at ca. 35.5° shifted toward higher or lower angles, and the lattice parameter a_0 significantly increased or decreased. This was ascribed to the difference in ionic radii among Fe^{2+}, Fe^{3+}, and substituting cations (Table 1). For example, the ionic radius of Zn^{2+} on the tetrahedral sites is

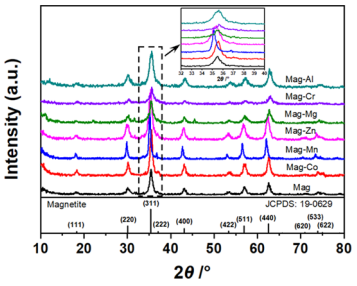

Figure 1. XRD patterns of $Fe_{3-x}M_xO_4$ samples and the standard card of magnetite (JCPDS: 19-0629).

0.060 nm, which is considerably larger than that of the tetrahedral Fe^{3+} (0.049 nm).[18] Therefore, the incorporation of Zn^{2+} into magnetite expanded the lattice and increased the lattice parameter. According to Bragg's law, the interplanar spacing *d* is negatively correlated with the diffraction angle 2θ.[30] Thus, the diffraction peaks shifted to a lower angle by Zn substitution.

The occupancy of substituting metals in the spinel structure of magnetite was analyzed by Mössbauer spectroscopy. For Mag, it consisted of hyperfine field (B_{hf}) of 47.9 T (tetrahedral site A) and 43.2 T (octahedral site B) with isomer shifts (IS) of 0.329 and 0.375 mm s^{-1}, respectively (Table S2). The IS value of B sites was lower than the theoretical value of octahedral Fe^{2+} and Fe^{3+} (0.600−0.700 mm s^{-1}),[24,31] which was ascribed to the oxidation of Mag in the synthesis and preservation. For Mag-Co and Mag-Mg, the relative area of B sites decreased from 64.9 (Mag) to 48.3 and 50.6%, respectively (Table S2 and Figure S1). This indicated the octahedral preference of Co^{2+} and Mg^{2+} in magnetite. Similar octahedral occupancy of Cr^{3+} and Al^{3+} was also confirmed in previous studies.[32,33] For Mag-Mn, the relative area of B sites (60.6%) was lower than that of Mag (64.9%) (Table S2 and Figure S1). According to previous studies,[22,34] the coexisting Mn^{2+} and Mn^{3+} in magnetite primarily occupied the octahedral sites with a minor amount occupying the tetrahedral sites, which was confirmed by the decrease of the relative area of B sites by Mn substitution. Based on the X-ray adsorption fine structure (XAFS) analysis in our previous study,[23] Zn^{2+} in Mag-Zn preferentially occupied the tetrahedral sites, accompanied with the oxidation of octahedral Fe^{2+} to Fe^{3+} to keep the charge balance.[18]

The above different occupancy of substituting ions gave rise to distinct surface properties of $Fe_{3-x}M_xO_4$ (Table 1). For example, most substitutions greatly altered the BET SSA of magnetite. The incorporation of Mg, Cr, Al, and Zn showed a positive effect on SSA, while Mn had a negative effect. The active sites are the active surface hydroxyls (≡FeOH) at the magnetite surface, which are amphoteric and can bind or release protons.[3,35] The active-site density of $Fe_{3-x}M_xO_4$ was calculated by the Gran function (Figure S2), which was in the range of (1.5−4.5) × 10^{20} site g^{-1}. The substitutions of Co, Mn, Zn, and Mg increased the active-site density, while Cr and Al decreased it. The pH_{pzc} of $Fe_{3-x}M_xO_4$ was similar, in the range of 6.7−7.1. Co, Mn, and Zn substitutions increased the electrical conductivity of magnetite, while Mg, Cr, and Al substitutions decreased it.

NB Reduction by $Fe_{3-x}M_xO_4$/$Fe(II)_{aq}$. In the presence of sole $Fe_{3-x}M_xO_4$ (Figure S3), ∼100% NB remained in solution. This suggested that NB could be neither adsorbed nor reduced by $Fe_{3-x}M_xO_4$. The lack of adsorption was attributed to the

https://dx.doi.org/10.1021/acsearthspacechem.0c00089
ACS Earth Space Chem. 2020, 4, 905−911

electrostatic repulsion between $Fe_{3-x}M_xO_4$ (pH_{pzc} in the range of 6.7−7.1) and NB (pK_a = −12.44) at pH 7.2,[36] while the invalid reduction was related to the low Fe^{2+} content in $Fe_{3-x}M_xO_4$.[23] In the presence of $Fe(II)_{aq}$ alone, NB was slowly reduced with the removal efficiency of ∼58.7% in 120 min (Figure 2). But NB reduction was significantly enhanced when

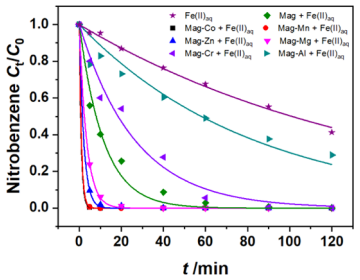

Figure 2. Reduction of nitrobenzene by $Fe_{3-x}M_xO_4/Fe(II)_{aq}$ systems and its fitting by a three-parameter single exponential decay model ($[Fe_{3-x}M_xO_4]_0$ = 1.0 g L^{-1}, $[Fe(II)_{aq}]_0$ = 2.0 mmol L^{-1}, $[NB]_0$ = 0.081 mmol L^{-1}, and pH = 7.2 ± 0.1).

magnetite coexisted with $Fe(II)_{aq}$. This indicated that the NB reduction by the magnetite/$Fe(II)_{aq}$ system was controlled by a heterogeneous process, where adsorbed Fe(II) acted as an electron donor. According to previous studies, the substance was reduced by structural Fe^{2+} in magnetite, where the oxidized magnetite was further recharged by adsorbed Fe(II).[4,10] Among $Fe_{3-x}M_xO_4/Fe(II)_{aq}$ systems, NB was completely reduced by Mag-Co/$Fe(II)_{aq}$, Mag-Mn/$Fe(II)_{aq}$, Mag-Zn/$Fe(II)_{aq}$, and Mag-Mg/$Fe(II)_{aq}$ in 40 min, and by Mag/$Fe(II)_{aq}$ and Mag-Cr/$Fe(II)_{aq}$ in 120 min. For Mag-Al/$Fe(II)_{aq}$, approximately 71.1% of NB was removed in 120 min (Figure 2). Thus, the substitutions of Co, Mn, Zn, and Mg promoted the reducibility of magnetite/$Fe(II)_{aq}$ system, while Cr and Al substitutions retarded the reactivity of the magnetite/$Fe(II)_{aq}$ system.

The reduction kinetics of NB was modeled using a three-parameter single exponential decay model ($R^2 \geq 0.91$, Text S2),[37] which was separated in two stages, i.e., an initially rapid reduction followed by a delayed reduction. The deceleration in the second stage was ascribed to the oxidation precipitation of Fe(II) on the magnetite surface, which formed a passivation layer blocking the active sites.[4] The k_{obs} value decreased as follows: Mag-Co/$Fe(II)_{aq}$ > Mag-Mn/$Fe(II)_{aq}$ > Mag-Zn/$Fe(II)_{aq}$ > Mag-Mg/$Fe(II)_{aq}$ > Mag/$Fe(II)_{aq}$ > Mag-Cr/$Fe(II)_{aq}$ > Mag-Al/$Fe(II)_{aq}$ (Table S3 and Figure 3). This further illustrated the positive roles of Co, Mn, Zn, and Mg substitutions on the reducibility of the magnetite/$Fe(II)_{aq}$ system.

During the reduction process, two intermediates, i.e., nitrosobenzene and hydroxylamine, were detected. They were quickly generated, but finally transformed to aniline (Figure S4). According to previous studies,[26,27] aniline is less toxic and more easily mineralized and biodegraded than NB. The mass balance of reaction products illustrated that NB was stoichiometrically reduced to aniline (Figure S4). The distribution of NB and its reduction products also reflected their difference in the reducing capacity of $Fe_{3-x}M_xO_4/Fe(II)_{aq}$ systems. For instance, within 40 min, almost 100% aniline was generated by the high reducing systems, Mag-Co/$Fe(II)_{aq}$ and Mag-Mn/$Fe(II)_{aq}$, but only 30.9% aniline was generated in the low-activity Mag-Al/$Fe(II)_{aq}$ system (Figure S4). Based on the

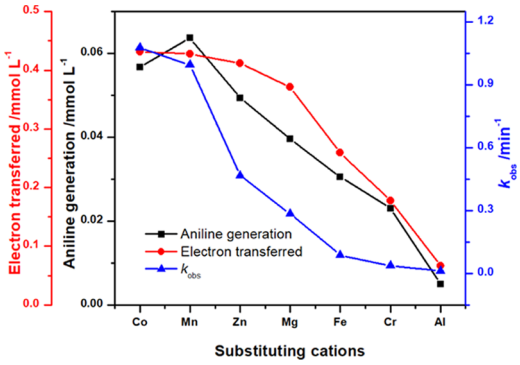

Figure 3. Effect of substitution cations on the aniline generation rate (10 min), extent of electron transfer (10 min), and reaction rate constant k_{obs}.

distribution of reduction products, the extent of electron transfer in $Fe_{3-x}M_xO_4/Fe(II)_{aq}$ systems was quantified (eq 2 and Figure 3). It displayed a similar variation trend to those of rate constant, k_{obs}, and aniline generation rate among $Fe_{3-x}M_xO_4/Fe(II)_{aq}$ systems (Figure 3).

$$[e^-]_t^{\text{transferred}} = 2[Ar - NO]_t + 4[Ar - NHOH]_t + 6[Ar - NH_2]_t \quad (2)$$

The variation of the $Fe(II)_{aq}$ concentration was also traced. Before the NB addition, the initial adsorption of $Fe(II)_{aq}$ in Mag, Mag-Co, Mag-Mn, Mag-Zn, Mag-Mg, Mag-Cr, and Mag-Al was 1.07, 1.48, 1.42, 1.36, 1.29, 0.82, and 0.79 mmol g^{-1}, respectively (Figure 4), which was linearly correlated to k_{obs}

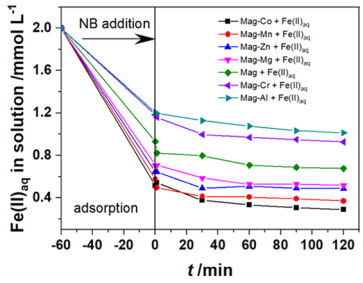

Figure 4. Variation of $Fe(II)_{aq}$ concentration versus reaction time ($[Fe_{3-x}M_xO_4]_0$ = 1.0 g L^{-1}, $[Fe(II)_{aq}]_0$ = 2.0 mmol L^{-1}, $[NB]_0$ = 0.081 mmol L^{-1}, and pH = 7.2 ± 0.1).

(R^2 = 0.89, Table 2). This indicated the vital role of adsorbed Fe(II) in the reduction reaction.[13] The adsorbed Fe(II) could reduce octahedral Fe^{3+} to octahedral Fe^{2+} in the underlying magnetite and recover the reducing capacity of magnetite.[4] Since the excess dissolved Fe(II) was not removed after the adsorption equilibrium, it could be readsorbed on magnetite and the oxidized magnetite could be reduced.[12,13] Thus, the $Fe(II)_{aq}$ concentration gradually decreased as the reduction process proceeded (Figure 4). With the reaction proceeding, the generated Fe(III) was precipitated on the $Fe_{3-x}Zn_xO_4$ surface and could not be detected in the solution.

Correlation Analysis. Based on the variation of physiochemical properties and microstructure of magnetite by substitution, and their activity toward NB reduction with $Fe(II)_{aq}$, the Pearson analysis was carried out to grasp the mechanism of metal substitution on the reducibility of

https://dx.doi.org/10.1021/acsearthspacechem.0c00089
ACS Earth Space Chem. 2020, 4, 905−911

Table 2. Related Matrix of Pearson Correlation Analysis for the Physiochemical Properties and Reactivities of Substituted Magnetite $Fe_{3-x}M_xO_4$[a]

	crystal size	specific surface area	active-site density	conductivity	pH_{pzc}	$Fe(II)_{aq}$ adsorption	rate constant (k_{obs})	election transferred
crystal size	1.000							
specific surface area	−0.974	1.000						
active-site density			1.000					
conductivity			0.873	1.000				
pH_{pzc}					1.000			
$Fe(II)_{aq}$ adsorption		−0.730	0.952	0.762		1.000		
rate constant k_{obs}			0.933	0.944		0.889	1.000	
election transferred			0.955	0.714		0.971	0.837	1.000

[a]Data are not shown owing to no significant correlation with each other ($P > 0.05$ and $R^2 < 0.50$).

magnetite/$Fe(II)_{aq}$ system and the controlling factors (Figure S5 and Table 2).

As observed in the NB reduction by $Fe_{3-x}M_xO_4/Fe(II)_{aq}$, the adsorption of $Fe(II)_{aq}$ was indispensable for the efficient reduction. Thus, in Pearson analysis, the reduction rate constant, i.e., k_{obs}, was closely related to the amount of Fe(II) adsorption ($R^2 = 0.89$). This was consistent with the study by Klausen et al.,[13] where k_{obs} increased with increasing $Fe(II)_{aq}$ concentration and leveled out as the adsorption of $Fe(II)_{aq}$ achieved saturation. For the amount of Fe(II) adsorption, it displayed a positive correlation with active-site density ($R^2 = 0.95$). According to the previous study,[13] $Fe(II)_{aq}$ was adsorbed on the magnetite surface via inner-sphere complexation rather than outer-sphere complexation and complexed with the deprotonated surface hydroxyls directly at the magnetite surface; therefore, the density of active surface hydroxyls determined the Fe(II) adsorption. The inner-sphere adsorbed Fe(II) facilitated the electron transfer to magnetite and environmental substances through conjugated electron orbits. This accounted for the vital role of $Fe(II)_{aq}$ adsorption for the reducibility of magnetite/$Fe(II)_{aq}$ system. Among the substituting metals, Mn, Co, Zn, and Mg increased the active-site density of magnetite and thus improved the adsorption of $Fe(II)_{aq}$, whereas Al and Cr showed a suppressing effect. Our previous study also showed that the metal substitutions constrained the active-site density of magnetite, resulting in the enhancement of Pb(II) adsorption on magnetite.[20] Theoretically, the adsorption of $Fe(II)_{aq}$ on the magnetite surface should be strongly dependent on pH. But in this study, the $Fe(II)_{aq}$ adsorption was found to be irrelevant to pH_{PZC} (6.7−7.1) of $Fe_{3-x}M_xO_4$. This was probably ascribed to the negligible effect of substitution on pH_{PZC} and the similar reaction pH (7.2) to pH_{PZC}. Specific surface area showed a negative correlation to crystal size, due to the fact that low crystallinity decreased crystal size and accordingly increased SSA. It was interesting to find the negative relationship between the amount of $Fe(II)_{aq}$ adsorption and SSA ($R^2 = -0.73$). This was probably ascribed to the steric hindrance effect during the Fe(II) complexation with magnetite particles with smaller size but larger SSA.

After the introduction of NB to the magnetite/$Fe(II)_{aq}$ system, NB was reduced by adsorbed Fe(II) and $Fe_{3-x}M_xO_4$. Thus, k_{obs} manifested positive correlation with not only the $Fe(II)_{aq}$ adsorption ($R^2 = 0.89$) but also the extent of electron transfer reaction ($R^2 = 0.84$). On the one hand, the electron transfer reaction was greatly constrained by the $Fe(II)_{aq}$ adsorption ($R^2 = 0.97$), indicating the critical role of adsorbed Fe(II) as an electron donor. Thus, the electron transfer reaction was also positively correlated to the active-site density ($R^2 = 0.96$), due to the close association between active-site density and the $Fe(II)_{aq}$ adsorption ($R^2 = 0.95$).

On the other hand, the electron transfer reaction was also affected by the conductivity of $Fe_{3-x}M_xO_4$ ($R^2 = 0.71$). This was explained by the electron transfer driven by bulk electron conduction.[38] In the magnetite/$Fe(II)_{aq}$ system, magnetite acted as a source/sink of electron in the coupled system, where electrons migrated both within the bulk structure and across the solid−water interface from magnetite to environmental substances.[4,14,15] Thus, the electron transfer process was mediated by conductivity, affecting the regeneration of active sites and the ongoing reduction reaction. Among the substituting metals, Mn, Co, and Zn significantly increased the conductivity of magnetite, while Mg, Cr, and Al showed an inhibition effect, owing to their chemical properties and microstructure in magnetite. The excellent conductivity of magnetite originated from the electron delocalization between octahedral Fe^{2+} and Fe^{3+}. Co and Mn occupied the octahedral sites and form large quantities of galvanic couples by coupling the thermodynamically favorable redox pairs Co^{2+}/Co^{3+}, Mn^{2+}/Mn^{3+}, and Fe^{2+}/Fe^{2+}, resulting in the acceleration of electron transfer and thus the increase of conductivity.[22,39] For Zn^{2+}, it primarily replaced the tetrahedral Fe^{3+}, together with the octahedral Fe^{2+} oxidation.[18,23] This increased the electron transfer reaction on the octahedral sites and thus enhanced the conductivity of magnetite. For Mg, Cr, and Al with unique valence fitting for the accommodation in the spinel structure (i.e., Mg^{2+}, Cr^{3+}, and Al^{3+}), they occupied the octahedral sites and decreased the structural Fe^{2+} or Fe^{3+} content, respectively, giving rise to the decrease in conductivity.

Based on the Pearson analysis, among the physicochemical properties of magnetite, active-site density and conductivity were the primary factors determining the effect of metal substitution on the reducibility of magnetite/$Fe(II)_{aq}$ system. The Co, Mn, and Zn substitutions increased both the active-site density and conductivity of magnetite, while Mg substitutions increased only the active-site density. This was also partially found in previous studies. For example, Co and Mn substitutions significantly increased the active-site density of magnetite and accordingly improved the adsorption capacity toward Pb(II).[20,22] Zn and Co substitutions generally promoted the reduction of (chloro)nitrobenzene via the enhancement of the conductivity of magnetite.[23,24] Co and Mn substitutions improved the Fenton reactivity of magnetite by accelerating the electron transfer in the magnetite structure.[16,21] Thus, the substitution of these metals benefited the reducing capacity of the magnetite/$Fe(II)_{aq}$ system in the

https://dx.doi.org/10.1021/acsearthspacechem.0c00089
ACS Earth Space Chem. 2020, 4, 905−911

order of Co > Mn > Zn > Mg. On the contrary, Cr and Al substitutions decreased both the active-site density and conductivity and thus suppressed the reducing capacity of the coupled system.

CONCLUSIONS

In the present study, NB was rapidly reduced by different substituted magnetite ($Fe_{3-x}M_xO_4$, M = Co^{2+}, Mn^{2+}, Zn^{2+}, Mg^{2+}, Cr^{3+}, and Al^{3+}) coupled with $Fe(II)_{aq}$. Both the reduction kinetics and the extent of electron transfer indicated that the substitution of divalent metals in magnetite significantly improved the reducing capacity of magnetite/$Fe(II)_{aq}$ system, while trivalent metals suppressed the reduction. These phenomena were attributed to the variation of the active-site density and conductivity of magnetite induced by substitutions. Co, Mn, and Zn substitutions increased both the active-site density and conductivity of magnetite, promoting the $Fe(II)_{aq}$ adsorption and electron transfer reaction in the system, while Cr and Al substitution operated in the reverse direction. The Mg substitution only increased the active-site density but slightly decreased conductivity. The obtained results will be helpful for better understanding of the effects of isomorphous substitution on the surface reactivity of magnetite and providing important clues for the application of natural magnetite to the anoxic remediation technology.

ASSOCIATED CONTENT

Supporting Information

The Supporting Information is available free of charge at https://pubs.acs.org/doi/10.1021/acsearthspacechem.0c00089.

Active-site density and pH_{PZC} analysis, kinetics analysis, chemical analysis, room-temperature Mössbauer parameters and spectra, Gran's curve of $Fe_{3-x}M_xO_4$ particles, degradation of nitrobenzene in the presence of $Fe_{3-x}M_xO_4$ alone, distribution of NB and its products during the reduction by $Fe_{3-x}M_xO_4/Fe(II)_{aq}$, and heat map of Pearson correlation analysis (PDF)

AUTHOR INFORMATION

Corresponding Author

Xiaoliang Liang − *CAS Key Laboratory of Mineralogy and Metallogeny/Guangdong Provincial Key Laboratory of Mineral Physics and Materials, Guangzhou Institute of Geochemistry, Chinese Academy of Sciences, Guangzhou 510640, P. R. China; Institutions of Earth Science, Chinese Academy of Sciences, Beijing 100029, P. R. China; University of Chinese Academy of Sciences, Beijing 100049, P. R. China;* orcid.org/0000-0001-6674-9354; Email: liangxl@gig.ac.cn

Authors

Ying Li − *CAS Key Laboratory of Mineralogy and Metallogeny/Guangdong Provincial Key Laboratory of Mineral Physics and Materials, Guangzhou Institute of Geochemistry, Chinese Academy of Sciences, Guangzhou 510640, P. R. China; Department of Natural Resources and Environmental Sciences, University of Illinois at Urbana-Champaign, Urbana, Illinois 61801, United States; University of Chinese Academy of Sciences, Beijing 100049, P. R. China*

Gaoling Wei − *Guangdong Key Laboratory of Integrated Agro-Environmental Pollution Control and Management, Guangdong Institute of Eco-Environmental Science & Technology, Guangzhou 510650, P. R. China; National-Regional Joint Engineering Research Center for Soil Pollution Control and Remediation in South China, Guangzhou 510650, P. R. China*

Caihua Zhang − *CAS Key Laboratory of Mineralogy and Metallogeny/Guangdong Provincial Key Laboratory of Mineral Physics and Materials, Guangzhou Institute of Geochemistry, Chinese Academy of Sciences, Guangzhou 510640, P. R. China*

Jianxi Zhu − *CAS Key Laboratory of Mineralogy and Metallogeny/Guangdong Provincial Key Laboratory of Mineral Physics and Materials, Guangzhou Institute of Geochemistry, Chinese Academy of Sciences, Guangzhou 510640, P. R. China; Institutions of Earth Science, Chinese Academy of Sciences, Beijing 100029, P. R. China; University of Chinese Academy of Sciences, Beijing 100049, P. R. China;* orcid.org/0000-0002-9002-4457

Yuji Arai − *Department of Natural Resources and Environmental Sciences, University of Illinois at Urbana-Champaign, Urbana, Illinois 61801, United States;* orcid.org/0000-0002-2560-7445

Complete contact information is available at: https://pubs.acs.org/10.1021/acsearthspacechem.0c00089

Notes

The authors declare no competing financial interest.

ACKNOWLEDGMENTS

This work was financially supported by the Key Research Program of Frontier Sciences, CAS (grant no. QYZDJ-SSW-DQC023), the National Natural Science Foundation of China (grant no. 41572032), the Guangdong Special Branch Plans (grant no. 201629015), Youth Innovation Promotion Association CAS (grant no. Y201863), and the Science and Technology Planning Project of Guangdong Province, China (grant no. 2017B030314175). This is contribution No. IS-2868 from GIGCAS.

REFERENCES

(1) Frierdich, A. J.; Catalano, J. G. Fe (II)-mediated reduction and repartitioning of structurally incorporated Cu, Co, and Mn in iron oxides. *Environ. Sci. Technol.* **2012**, *46*, 11070−11077.

(2) Stewart, S. M.; Hofstetter, T. B.; Joshi, P.; Gorski, C. A. Linking thermodynamics to pollutant reduction kinetics by Fe^{2+} bound to iron oxides. *Environ. Sci. Technol.* **2018**, *52*, 5600−5609.

(3) Cornell, R. M.; Schwertmann, U. *The Iron Oxides: Structure, Properties, Reactions, Occurrence, and Uses*, 2nd ed.; John Wiley & Sons, 2003.

(4) Gorski, C. A.; Scherer, M. M. Influence of magnetite stoichiometry on Fe^{II} uptake and nitrobenzene reduction. *Environ. Sci. Technol.* **2009**, *43*, 3675−3680.

(5) Haderlein, S. B.; Pecher, K. Pollutant Reduction In Heterogeneous Fe(II)-Fe(III) systems. In *Mineral-Water Interfacial Reactions*; American Chemical Society, 1999; Vol. *715*, pp 342−357.

(6) Usman, M.; Byrne, J. M.; Chaudhary, A.; Orsetti, S.; Hanna, K.; Ruby, C.; Kappler, A.; Haderlein, S. B. Magnetite and green rust: Synthesis, properties, and environmental applications of mixed-valent iron minerals. *Chem. Rev.* **2018**, *118*, 3251−3304.

(7) Vikesland, P. J.; Heathcock, A. M.; Rebodos, R. L.; Makus, K. E. Particle size and aggregation effects on magnetite reactivity toward carbon tetrachloride. *Environ. Sci. Technol.* **2007**, *41*, 5277−5283.

(8) Cutting, R. S.; Coker, V. S.; Telling, N. D.; Kimber, R. L.; Pearce, C. I.; Ellis, B. L.; Lawson, R. S.; Van der Laan, G.; Pattrick, R. A. D.; Vaughan, D. J.; Arenholz, E.; Lloyd, J. R. Optimizing Cr(VI) and Tc(VII) remediation through nanoscale biomineral engineering. *Environ. Sci. Technol.* **2010**, *44*, 2577−2584.

(9) Pasakarnis, T. S.; Boyanov, M. I.; Kemner, K. M.; Mishra, B.; O'Loughlin, E. J.; Parkin, G.; Scherer, M. M. Influence of chloride and Fe(II) content on the reduction of Hg(II) by magnetite. *Environ. Sci. Technol.* **2013**, *47*, 6987−6994.
(10) Latta, D. E.; Gorski, C. A.; Boyanov, M. I.; O'Loughlin, E. J.; Kemner, K. M.; Scherer, M. M. Influence of magnetite stoichiometry on U^{VI} reduction. *Environ. Sci. Technol.* **2012**, *46*, 778−786.
(11) Vermeire, M.-L.; Bonneville, S.; Stenuit, B.; Delvaux, B.; Cornélis, J.-T. Is microbial reduction of Fe (III) in podzolic soils influencing C release? *Geoderma* **2019**, *340*, 1−10.
(12) Marsac, R.; Pasturel, M.; Hanna, K. Reduction kinetics of nitroaromatic compounds by titanium-substituted magnetite. *J. Phys. Chem. C* **2017**, *121*, 11399−11406.
(13) Klausen, J.; Troeber, S. P.; Haderlein, S. B.; Schwarzenbach, R. P. Reduction of substituted nitrobenzenes by Fe(II) in aqueous mineral suspensions. *Environ. Sci. Technol.* **1995**, *29*, 2396−2404.
(14) Peng, H.; Pearce, C. I.; Huang, W.; Zhu, Z.; N'Diaye, A. T.; Rosso, K. M.; Liu, J. Reversible Fe(II) uptake/release by magnetite nanoparticles. *Environ. Sci.: Nano* **2018**, *5*, 1545−1555.
(15) Peng, H.; Pearce, C. I.; N'Diaye, A. T.; Zhu, Z.; Ni, J.; Rosso, K. M.; Liu, J. Redistribution of electron equivalents between magnetite and aqueous Fe^{2+} induced by a model quinone compound AQDS. *Environ. Sci. Technol.* **2019**, *53*, 1863−1873.
(16) Zhong, Y.; Liang, X.; He, Z.; Tan, W.; Zhu, J.; Yuan, P.; Zhu, R.; He, H. The constraints of transition metal substitutions (Ti, Cr, Mn, Co and Ni) in magnetite on its catalytic activity in heterogeneous Fenton and UV/Fenton reaction: From the perspective of hydroxyl radical generation. *Appl. Catal., B* **2014**, *150−151*, 612−618.
(17) Nadoll, P.; Angerer, T.; Mauk, J. L.; French, D.; Walshe, J. The chemistry of hydrothermal magnetite: A review. *Ore Geol. Rev.* **2014**, *61*, 1−32.
(18) Byrne, J. M.; Coker, V. S.; Cespedes, E.; Wincott, P. L.; Vaughan, D. J.; Pattrick, R. A. D.; van der Laan, G.; Arenholz, E.; Tuna, F.; Bencsik, M.; Lloyd, J. R.; Telling, N. D. Biosynthesis of zinc substituted magnetite nanoparticles with enhanced magnetic properties. *Adv. Funct. Mater.* **2014**, *24*, 2518−2529.
(19) Schwertmann, U.; Murad, E. The influence of aluminum on iron oxides: XIV. Al-substituted magnetite synthesized at ambient temperatures. *Clays Clay Miner.* **1990**, *38*, 196−202.
(20) Liang, X.; Wei, G.; Xiong, J.; Tan, F.; He, H.; Qu, C.; Yin, H.; Zhu, J.; Zhu, R.; Qin, Z.; Zhang, J. Adsorption isotherm, mechanism, and geometry of Pb(II) on magnetites substituted with transition metals. *Chem. Geol.* **2017**, *470*, 132−140.
(21) Costa, R. C. C.; Lelis, M. F. F.; Oliveira, L. C. A.; Fabris, J. D.; Ardisson, J. D.; Rios, R. R. V. A.; Silva, C. N.; Lago, R. M. Novel active heterogeneous Fenton system based on $Fe_{3-x}M_xO_4$ (Fe, Co, Mn, Ni): The role of M^{2+} species on the reactivity towards H_2O_2 reactions. *J. Hazard. Mater.* **2006**, *129*, 171−178.
(22) Liang, X.; He, Z.; Wei, G.; Liu, P.; Zhong, Y.; Tan, W.; Du, P.; Zhu, J.; He, H.; Zhang, J. The distinct effects of Mn substitution on the reactivity of magnetite in heterogeneous Fenton reaction and Pb(II) adsorption. *J. Colloid Interface Sci.* **2014**, *426*, 181−189.
(23) Li, Y.; Wei, G.; He, H.; Liang, X.; Chu, W.; Huang, D.; Zhu, J.; Tan, W.; Huang, Q. Improvement of zinc substitution in the reactivity of magnetite coupled with aqueous Fe(II) towards nitrobenzene reduction. *J. Colloid Interface Sci.* **2018**, *517*, 104−112.
(24) Liang, X.; Li, Y.; Wei, G.; He, H.; Stucki, J. W.; Ma, L.; Pentrakova, L.; Pentrak, M.; Zhu, J. Heterogeneous reduction of 2-chloronitrobenzene by Co-substituted magnetite coupled with aqueous Fe^{2+}: Performance, factors, and mechanism. *ACS Earth Space Chem.* **2019**, *3*, 728−737.
(25) Dupuis, C.; Beaudoin, G. Discriminant diagrams for iron oxide trace element fingerprinting of mineral deposit types. *Miner. Deposita* **2011**, *46*, 319−335.
(26) Zhang, J.; Zhang, Y.; Quan, X. Bio-electrochemical enhancement of anaerobic reduction of nitrobenzene and its effects on microbial community. *Biochem. Eng. J.* **2015**, *94*, 85−91.
(27) Wang, A.-J.; Cheng, H.-Y.; Liang, B.; Ren, N.-Q.; Cui, D.; Lin, N.; Kim, B.-H.; Rabaey, K. Efficient reduction of nitrobenzene to aniline with a biocatalyzed cathode. *Environ. Sci. Technol.* **2011**, *45*, 10186−10193.
(28) Li, Y.; Wei, G.; Zhang, C.; Liang, X.; Chu, W.; He, H.; Stucki, J. W.; Ma, L.; Lin, X.; Zhu, J. Remarkable effect of Co substitution in magnetite on the reduction removal of Cr(VI) coupled with aqueous Fe(II): Improvement mechanism and Cr fate. *Sci. Total Environ.* **2019**, *656*, 400−408.
(29) Tamura, H.; Goto, K.; Yotsuyanagi, T.; Nagayama, M. Spectrophotometric determination of iron(II) with 1,10-phenanthroline in the presence of large amounts of iron(III). *Talanta* **1974**, *21*, 314−318.
(30) Kacher, J.; Landon, C.; Adams, B. L.; Fullwood, D. Bragg's Law diffraction simulations for electron backscatter diffraction analysis. *Ultramicroscopy* **2009**, *109*, 1148−1156.
(31) Gorski, C. A.; Scherer, M. M. Determination of nanoparticulate magnetite stoichiometry by Mössbauer spectroscopy, acidic dissolution, and powder X-ray diffraction: A critical review. *Am. Mineral.* **2010**, *95*, 1017−1026.
(32) Rosenberg, M.; Deppe, P.; Janssen, H. U.; Brabers, V. A. M.; Li, F. S.; Dey, S. A Mössbauer study of Al and Ga substituted magnetite. *J. Appl. Phys.* **1985**, *57*, 3740−3742.
(33) Liang, X.; Zhong, Y.; He, H.; Yuan, P.; Zhu, J.; Zhu, S.; Jiang, Z. The application of chromium substituted magnetite as heterogeneous Fenton catalyst for the degradation of aqueous cationic and anionic dyes. *Chem. Eng. J.* **2012**, *191*, 177−184.
(34) Denecke, M. A.; Gunßer, W.; Buxbaum, G.; Kuske, P. Manganese valence in precipitated manganese ferrite. *Mater. Res. Bull.* **1992**, *27*, 507−514.
(35) Jolsterå, R.; Gunneriusson, L.; Holmgren, A. Surface complexation modeling of Fe_3O_4−H^+ and Mg(II) sorption onto maghemite and magnetite. *J. Colloid Interface Sci.* **2012**, *386*, 260−267.
(36) Zhao, Z.; Sun, W.; Yang, X.; Ye, X.; Wu, Y. Study of the catalytic behaviors of concentrated heteropolyacid solution. I. A novel catalyst for isobutane alkylation with butenes. *Catal. Lett.* **2000**, *65*, 115−121.
(37) Lin, K.; Ding, J.; Huang, X. Debromination of tetrabromobisphenol A by nanoscale zerovalent iron: Kinetics, influencing factors, and pathways. *Ind. Eng. Chem. Res.* **2012**, *51*, 8378−8385.
(38) Latta, D. E.; Gorski, C. A.; Scherer, M. M. Influence of Fe^{2+}-catalysed iron oxide recrystallization on metal cycling. *Biochem. Soc. Trans.* **2012**, *40*, 1191−1197.
(39) Li, X.; Wang, Z.; Zhang, B.; Rykov, A. I.; Ahmed, M. A.; Wang, J. $Fe_xCo_{3-x}O_4$ nanocages derived from nanoscale metal-organic frameworks for removal of bisphenol A by activation of peroxymonosulfate. *Appl. Catal., B* **2016**, *181*, 788−799.
(40) Sidhu, P. S.; Gilkes, R. J.; Posner, A. M. The synthesis and some properties of Co, Ni, Zn, Cu, Mn and Cd substituted magnetites. *J. Inorg. Nucl. Chem.* **1978**, *40*, 429−435.
(41) Pistoia, G.; Antonini, A.; Rosati, R.; Bellitto, C.; Ingo, G. M. Doped Li-Mn spinels: Physical/chemical characteristics and electrochemical performance in Li batteries. *Chem. Mater.* **1997**, *9*, 1443−1450.
(42) Shannon, R. D. Revised effective ionic radii and systematic studies of interatomic distances in halides and chalcogenides. *Acta Crystallogr., Sect. A* **1976**, *32*, 751−767.
(43) Zhong, Y.; Liang, X.; Tan, W.; Zhong, Y.; He, H.; Zhu, J.; Yuan, P.; Jiang, Z. A comparative study about the effects of isomorphous substitution of transition metals (Ti, Cr, Mn, Co and Ni) on the UV/Fenton catalytic activity of magnetite. *J. Mol. Catal. A: Chem.* **2013**, *372*, 29−34.

https://dx.doi.org/10.1021/acsearthspacechem.0c00089
ACS Earth Space Chem. 2020, 4, 905−911